Dielectric permittivity of water confined in stacks of charged lipid layers: extracting profiles from molecular dynamics simulations using a modified Poisson-Boltzmann equation

Ludovic Gardré,[1] Swen Helstroffer,[2] Pierre Muller,[2] Fabrice Thalmann,[2] Thierry Charitat,[2] Laurent Joly,[1] and Claire Loison[1]

[1] *Université Claude Bernard Lyon 1, CNRS, Institut Lumière Matière, UMR5306, Villeurbanne, France*

[2] *UPR 22/CNRS, Institut Charles Sadron, Université de Strasbourg, 23 rue du Loess, BP 84047 67034 Strasbourg Cedex 2, France*

Abstract — Most organic and inorganic surfaces (e.g., glass, nucleic acids or lipid membranes) become charged in aqueous solutions. The resulting ionic distribution induces effective interactions between the charged surfaces. Stacks of like-charged lipid bilayers immersed in multivalent ion solutions exhibit strong coupling (SC) effects, where ion correlations cause counter-intuitive membrane attraction. A similar attraction observed with monovalent ions is explained by SC theory through reduced dielectric permittivity under confinement. To explore this phenomenon, we propose a modified Poisson-Boltzmann (mPB) model with spatially varying dielectric permittivity and explicit Born solvation energy for ions. We use the model to investigate the dielectric permittivity profile of confined water in molecular dynamics simulations of charged lipid layers stacks at varying hydration levels, and compare the results with alternative computational methods. The model captures a sharp decrease in permittivity as the system enters the attractive regime, converging to a plateau value that we attribute to lipid headgroups. The generic nature of the mPB framework allows application to other systems, such as other biological interfaces or solid walls, provided ions follow Boltzmann statistics.

Keywords — Confined water, dielectric permittivity, lipid layers, molecular dynamics

I. INTRODUCTION

Water is a crucial component of the human body, constituting over half of its composition[1]. In this complex biological system, water exists in confined spaces such as blood capillaries, within cells, or trapped between lipid membranes where it has been extensively studied[2]. Confined water exhibits properties significantly different from those in bulk[3]. The dielectric permittivity in particular is one of these properties. This macroscopic property of a continuous medium describes how it becomes polarized under an external electric field. The polarization arises from the complex microscopic polarization mechanisms within the medium and generally exhibits non-local behaviour. In bulk water, its value tends to be high due to the polar nature of the molecule. However, when confined, water does not have the freedom to rearrange its structure, thus resulting in a decrease of its dielectric permittivity[4].

Electrostatic interactions often govern biological dynamics in the vicinity of membranes[5] (e.g., the binding of proteins to the membranes). Therefore, studying confined water dielectric permittivity is really important to better understand the functioning of living bodies. Furthermore, biological systems generally contain many ions that play an important role in these electrostatic interactions. Depending on the nature of these ions, their number or the system configuration, there can be strong correlation effects between them.

To determine whether these correlation effects must be taken into account, one can compute the coupling constant Ξ of the ions confined between membranes with a given surface charge density σ_{s} as follows[6]:

$$\Xi = 2\pi q^3 \ell_{\mathrm{B}}^2 \frac{\sigma_{\mathrm{s}}}{e}\,, \tag{1}$$

where e is the elementary charge, q is the valence of the ions and ℓ_{B} is the Bjerrum length (the characteristic length at which the thermal energy equals the electrostatic interaction energy between two monovalent ions), given by[7]:

$$\ell_{\mathrm{B}} = \frac{\beta e^2}{4\pi\varepsilon_0\varepsilon_r}\,, \tag{2}$$

where ε_0 is the dielectric permittivity of the vacuum, ε_r is the relative dielectric permittivity of the solvent and $\beta = (k_B T)^{-1}$ with k_B the Boltzmann constant and T the temperature.

Low Ξ values correspond to a weak coupling regime where mean-field theories, like the Poisson-Boltzmann model, are adequate. However, these models tend to fail in a strong coupling (SC) regime, i.e. for high Ξ values. SC regime can lead to counter-intuitive phenomena, such as the attraction between stacks of identically charged lipid layers observed by Komorowski and al. in the presence of multivalent counterions[8]. Depending on the system configuration, SC theory can predict such attraction for Ξ values as low as 10. In the system of Ref. 8, due to the large valence of the ions, Ξ was estimated to

be on the order of 20 (assuming a water dielectric constant of 80), so that SC theory succeeded at explaining the attraction.

However, a similar attraction has been experimentally observed by Mukhina and al., this time in the presence of monovalent counterions[9]. In that situation, it is only possible to have $\Xi > 10$ by assuming that the dielectric constant of confined water is strongly reduced. For this reason, in the case of monovalent counterions the attraction between identically charged surfaces is perceived as the signature of a strong decrease in the dielectric constant of the confined water[10].

Though it is experimentally challenging[4,11] to probe the dielectric permittivity in these regions, numerical simulations can give good insights of its value. Using the fluctuation-dissipation theorem, Schlaich and al. have shown that one can compute the parallel and perpendicular components of the dielectric permittivity in inhomogeneous systems with no free charges[12]. Unfortunately, because of this restriction, this method cannot be applied to study confined water in systems containing ions, such as charged lipid membranes, which are very abundant in biology.

In this paper, we present an alternative approach to extract an effective dielectric permittivity profile of water confined between stacks of charged lipid membranes, *ie.* in the presence of free charges. Our method uses molecular dynamics (MD) simulations and is based on a mean-field approximation with the use of a modified Poisson-Boltzmann (mPB) equation. These modifications combine an effective local z-dependant dielectric permittivity[13] with the addition of a solvation energy term in the Boltzmann distribution of the ions[14].

In a first part, we present the systems we studied, the details of the model and the methods we used to calibrate and solve it. We then apply our model to investigate the value of the dielectric permittivity of water confined in stacks of charged lipid layers, in the presence of a monovalent salt. We present its results for a large range of hydration level of the lipid membranes, which allow to extract a dielectric permittivity at the centre of the confined water, at each hydration value. We then compare our approach to alternative ways of estimating the dielectric permittivity in such systems.

II. METHODS

A. Studied systems and molecular dynamics simulations

The systems studied in this work were all built from the same base elements: a lipid bilayer made of 1,2-dipalmitoyl-sn-glycero-3-phosphoserine (DPPS, negatively charged) solvated in water. We neutralized the charge of the lipids with Na^+ counterions. In addition, to test our model in presence of both cations and anions,

we included NaCl salt in the solvent, at a concentration of approximatively $0.25\,M$.

The amount of water plays an important role in these systems. It was controlled at the creation step by setting a hydration number (HN), corresponding to the number of water molecules per lipid (e.g., HN = 20 means there are 20 water molecules per lipid).

Depending on its hydration and temperature, the bilayer can be in the fluid or the gel phase. Fig. 1 shows example systems at HN = 35 and at two different temperatures. At the highest temperature, the bilayer is in the fluid phase and consequently the lipids are disordered. At the lowest temperature, the bilayer is in the gel phase. In this phase, the lipid tails are ordered, but not their heads.

Due to the structural difference between these two phases, the membrane has a different thickness which influences the box length in the z direction, meaning that L_z is not the same in all systems and varies depending on the physico-chemical conditions (e.g., T, HN, etc.).

The systems are considered symmetrical with respect to the plane defined by $z = z_{\max}$. In practice, when computing charge densities from MD simulations, the centre of mass of the bilayer is placed at the centre of the simulation box (in Fig. 1, this is equivalent to shifting the simulation box by $L_z/2$ in the z direction). The densities are then integrated along the z axis, then symmetrized and centred with respect to the bilayer centre of mass.

For HN > 10, all systems were built using charmm-gui[15]. This tool provided pre-equilibrated systems with bilayers in the fluid phase. In these systems, the bilayer was made of two leaflets of 100 lipids. At lower HN, to keep the salt concentration constant while still having a statistically relevant number of ions in the system, we quadrupled the systems size so each leaflet of the bilayer contained 400 lipids. These bigger systems were built iteratively: for each HN, we started by replicating the system at the HN just above (e.g., we replicated the HN = 11 system to create the HN = 10 system, and so on down to HN = 02). We then randomly removed water molecules and/or ions to match the desired HN, and salt concentration.

Regarding the force fields, we chose CHARMM36[16] for the lipid atoms. For water, we used TIP3P[17] for historical reasons, as CHARMM36 was originally developed with this forcefield. Dealing solely with monovalent counterions, we have neglected the polarization. We have not used explicit polarizable force fields[18], nor scaled-charge force fields[19]. These may be considered if one would extend this study to systems containing multivalent ions[20].

Short-ranged Van der Waals interactions were modelled with a Lennard-Jones potential. A cutoff distance was set at $12\,Å$, and we smoothly switched forces to 0 between 10 and $12\,Å$. We used Lorentz-Berthelot combination rules to compute the cross-species parameters. Long ranged Coulombic interactions were computed with the Particle-Mesh Ewald method. All simulations were
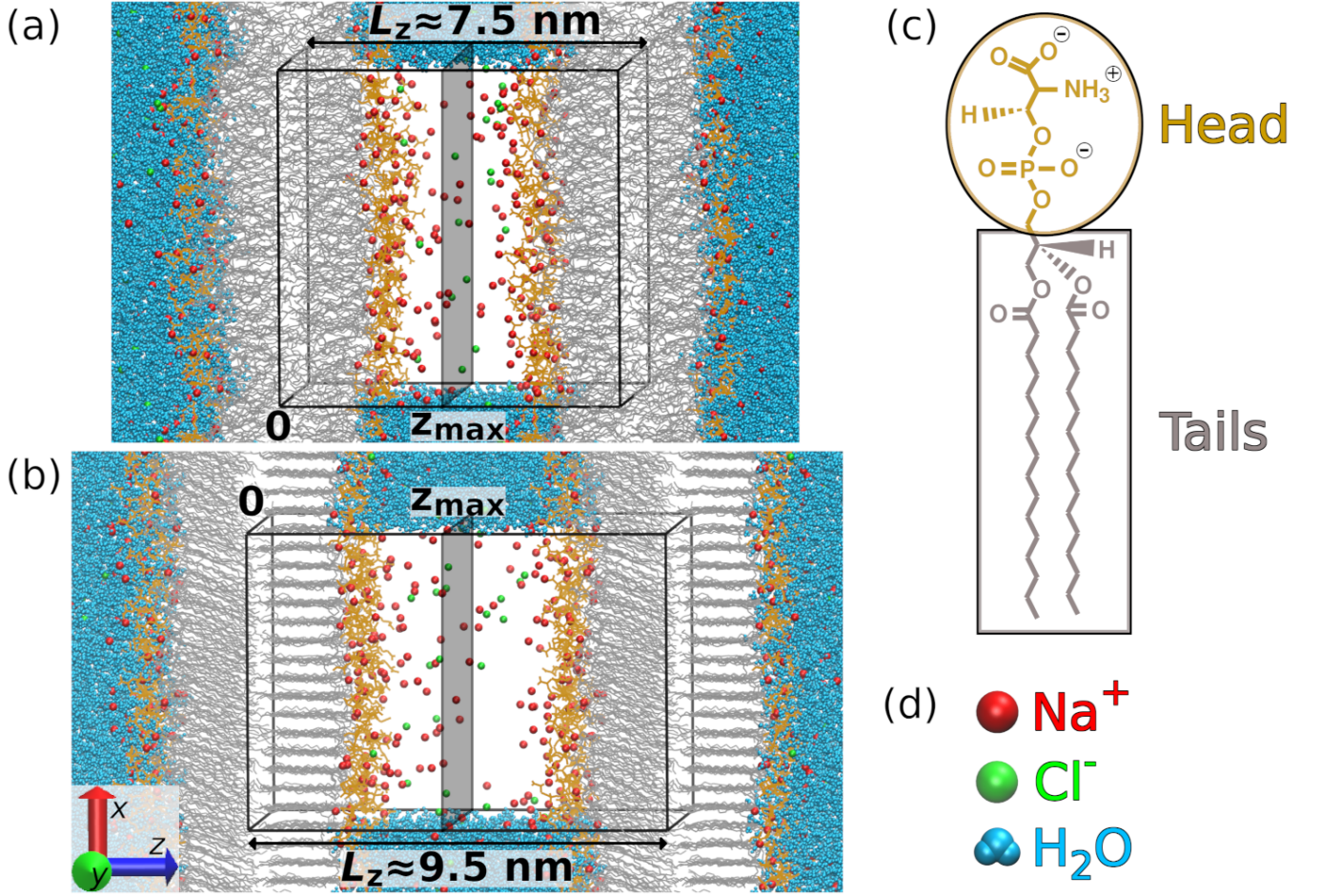
FIG. 1. (a, b) Snapshots of systems at HN = 35, respectively at $T = 353.15\,\mathrm{K}$ (bilayer in the fluid phase) and $T = 333.15\,\mathrm{K}$ (bilayer in the gel phase). The black boxes represent the simulation boxes, replicated in all directions of space. For clarity, the lipids' hydrogen atoms are not drawn in the snapshots, nor are water molecules in the simulation boxes. The z coordinate is set 0 at the centre of the left bilayer. It reaches $z_{\max} = L_z/2$ at the middle of the interlayer water. (c) Detail of the DPPS lipid molecule. The gold and silver colours respectively correspond to the heads and the tails of the lipids as drawn in the snapshots. (d) Interlayer species.

carried with a time step of $2\,\mathrm{fs}$, using Gromacs 2021.2 with CUDA support[21].

Every system was initially equilibrated at $T = 333.15\,\mathrm{K}$ before running the production simulations. The temperature was maintained with a Nosé-Hoover thermostat. We applied a pressure of 1 bar on the systems with two Parrinello-Rahman barostats. The first one controlled the normal pressure P_z, along the z direction. The other one controlled the coupled tangential pressures P_x and P_y, along the x and y directions, with the following constraint on the sides of the simulation box: $L_x = L_y$. We kept the surface tension of the bilayer null, meaning that:

$$P_z = \frac{P_x + P_y}{2}. \tag{3}$$

For each system, after the first production simulation at $T = 333.15\,\mathrm{K}$, we varied the temperature up to $T = 353.15\,\mathrm{K}$ with a step of 5 K. For every temperature,

we initially ran a $1\,\mu\mathrm{s}$ simulation. As expected, depending on the HN and temperature, we observed spontaneous phase transitions from fluid to gel (or vice versa). When it occurred, we extended the simulation length and discarded everything before the transition. Therefore, all observables shown in this work were computed over $1\,\mu\mathrm{s}$ phase-transition-free simulations.

B. Modified Poisson-Boltzmann model

The purpose of this work is to establish a method to obtain, from MD simulations, an effective profile of the dielectric permittivity of the ion-carrying water confined between charged lipid membranes. To do so, we propose to modify the Poisson-Boltzmann equation, a mean-field approximation that describes how electrolyte solutions behave in the vicinity of a charged interface.[22]

First, let us recall the standard Poisson-Boltzmann model, starting from Maxwell-Gauss equation in matter:

$$\boldsymbol{\nabla} \cdot \boldsymbol{D} = \rho_{\text{free}} \,, \tag{4}$$

where $\boldsymbol{D}$ is the electric displacement field and ρ_{free} is the free-charge density. From here, considering a planar geometry (with the z axis perpendicular to the plane), one can reduce the problem to one dimension thanks to the symmetries and invariances of the system:

$$-\varepsilon_0 \varepsilon_\perp \frac{\mathrm{d}^2 V}{\mathrm{d}z^2} = \rho_{\text{free}}(z) = \rho_{\text{ions}}(z) \,, \tag{5}$$

where $\varepsilon_\perp$ is the perpendicular component of the relative permittivity (assumed homogeneous) given by the relation $\boldsymbol{D}_\perp = \varepsilon_\perp \boldsymbol{E}_\perp$, and considering the total free-charge density is equal to the charge density of the ions ρ_{ions}. Using a Boltzmann distribution of cations and anions:

$$\rho_\pm(z) = \pm e C_{\text{salt}} \exp \left[\mp \beta e V(z) \right] \,, \tag{6}$$

where C_{salt} is the ions concentration in a reservoir, where V vanishes. One can express ρ_{ions} as follows:

$$\begin{aligned} \rho_{\text{ions}}(z) &= \rho_+(z) + \rho_-(z) \\ &= e C_{\text{salt}} \Big\{ \exp \Big[-\beta e V(z) \Big] \\ &\quad - \exp \Big[\beta e V(z) \Big] \Big\} \,. \end{aligned} \tag{7}$$

Combining Eq. (5) and Eq. (7), one gets the standard 1D Poisson-Boltzmann equation:

$$\frac{\mathrm{d}^2 V}{\mathrm{d}z^2} = \frac{2 e C_{\text{salt}}}{\varepsilon_0 \varepsilon_\perp} \sinh \left[\beta e V(z) \right] \,. \tag{8}$$

Introducing the dimensionless reduced electric potential ϕ, defined as $\phi(z) = \beta e V(z)$, and the Debye length λ_{D} (the characteristic length at which the electrolyte solution screens the electric field):

$$\lambda_{\text{D}} = \sqrt{\frac{\varepsilon_0 \varepsilon_\perp}{2 \beta e^2 C_{\text{salt}}}} \,, \tag{9}$$

one can rewrite Eq. (8) as:

$$\frac{\mathrm{d}^2 \phi}{\mathrm{d}z^2} = \frac{1}{\lambda_{\text{D}}^2} \sinh \left[\phi(z) \right] \,. \tag{10}$$

In our modified Poisson-Boltzmann (mPB) model, we allowed the relative permittivity $\varepsilon_\perp$ to vary along the z axis[13]. In addition, we included the lipid heads charge density ρ_{lipids} as a fixed external contribution to the total free-charge density. We then rewrote Eq. (5) as follows:

$$\begin{aligned} -\varepsilon_0 \frac{\mathrm{d}}{\mathrm{d}z} \left[\varepsilon_\perp(z) \frac{\mathrm{d}V(z)}{\mathrm{d}z} \right] &= \rho_{\text{free}}(z) \\ &= \rho_{\text{lipids}}(z) + \rho_{\text{ions}}(z). \end{aligned} \tag{11}$$

Since $\varepsilon_\perp$ varies with z, so does the ions solvation energy. We then introduced the solvation energy $W_\pm$ in the Boltzmann factor, using the Born expression[14]:

$$W_\pm(z) = \frac{e^2}{8 \pi \varepsilon_0 r_\pm} \left(\frac{1}{\varepsilon_\perp(z)} - \frac{1}{\varepsilon_\perp^{\text{ref}}} \right) \,, \tag{12}$$

where $r_\pm$ is the radius of the ion and $\varepsilon_\perp^{\text{ref}}$ is a reference value for the relative permittivity of water (e.g., bulk water value). The values of these parameters will be discussed in section II D, devoted to the model calibration. In the end, the ions charge density became:

$$\begin{aligned} \rho_{\text{ions}}(z) &= \rho_+(z) + \rho_-(z) \\ &= e C_{\text{salt}} \\ &\quad \times \Big\{ \exp \Big[-\beta W_+(z) - \beta e V(z) \Big] \\ &\qquad - \exp \Big[-\beta W_-(z) + \beta e V(z) \Big] \Big\} \,. \end{aligned} \tag{13}$$

C. Solving the mPB model's equation

In this section, we introduce the method we followed to solve the mPB model shown in Eq. (11). In this equation, the ions charge density ρ_{ions} is given by the analytical expression from Eq. (13), while the lipid charge density ρ_{lipids} corresponds to values extracted from MD simulations beforehand. These values were centred and symmetrized around the centre of mass of the bilayer, allowing to focus on one single half of the system when solving the equation. Therefore, we set the origin of the z axis at the centre of the bilayer and the maximum z value then corresponded to the centre of the interlayer water channel.

There were two unknown profiles in the equation: the electric potential $V(z)$ and the relative permittivity $\varepsilon_\perp(z)$. We chose to model the latter with a parametrized curve. This led to having only one fully unknown profile, the electric potential, so we could numerically solve the equation.

To decide on the shape of the dielectric permittivity profile, we analysed a system made of a zwitterionic lipid bilayer and no ions, i.e. without any free charges. In this situation, the electric displacement field is constant in the solvent, and the dielectric response can be obtained as the linear response of the polarization density upon the perturbation of an electric field. Fluctuation-dissipation approaches can then be used to extract a dielectric permittivity profile from the local dipole moment fluctuations in equilibrium simulations[12]. We used MAICoS (https://www.maicos-analysis.org), which provided us a profile of $\varepsilon_\perp^{-1}(z)$ that was close to a sigmoid. With the hypothesis that the shape of the dielectric permittivity profile would be roughly similar in a system with free charges, we chose to model its inverse (to stay consistent with the reference provided by MAICoS) using one

sigmoid and one gaussian, to allow for more degrees of freedom:

$$\varepsilon_\perp^{-1}\left(z, z_1, K, \sigma, \mu, C, \varepsilon_\perp^{\text{tails}}, \varepsilon_\perp^{\text{plateau}}\right)$$
$$= \frac{1}{\varepsilon_\perp^{\text{plateau}}} + \left(\frac{1}{\varepsilon_\perp^{\text{tails}}} - \frac{1}{\varepsilon_\perp^{\text{plateau}}}\right)$$
$$\times \frac{1}{1 + \exp\left[K\left(z - z_1\right)\right]} \quad (14)$$
$$+ \frac{C}{\sigma\sqrt{2\pi}} \exp\left[-\frac{(z - \mu)^2}{2\sigma^2}\right].$$

z_1 and K are parameters for the sigmoid component: the first one controls the coordinate of the sigmoid's inflection point while the other one controls its stiffness. σ, μ and C are parameters for the Gaussian component. The first two respectively correspond to its standard deviation and its expected value, while C controls its height. Finally, $\varepsilon_\perp^{\text{tails}}$ and $\varepsilon_\perp^{\text{plateau}}$ respectively control the left and the right horizontal asymptotes. An example of this curve is shown in Fig. S8 in the supplementary material.

Since we parametrized the inverse of the dielectric permittivity, we modified Eq. (11) to obtain an equation depending on $\varepsilon_\perp^{-1}$ and its derivative with respect to z. The complete system of equations numerically solved is given in section S-I in the supplementary material.

In this solving process, we added an optimization procedure, to obtain the best values for the parameters of $\varepsilon_\perp^{-1}$ (Eq. (14)). To do so, we fitted the ionic charge densities computed with Eq. (13) on the ionic charge densities extracted from the MD simulation.

D. Calibrating the mPB model

The calibration process served the purpose of fixing the value of two parameters: C_{salt} and $\varepsilon_\perp^{\text{ref}}$.

Three parameters were set prior to the calibration: the ionic radii of Na$^+$ and Cl$^-$ and the asymptotic value for the relative permittivity in the lipid tails $\varepsilon_\perp^{\text{tails}} = 2$. For the radii, we used the Born radii of these ions calculated from their free energies of hydration by Schmid and al.[23]: $r_+ = 0.187\,\text{nm}$ and $r_- = 0.186\,\text{nm}$.

We calibrated the model for each of the five temperatures. Every calibration was realised in two stages, using the HN = 45 system which contained enough water to have a solvent reservoir between the membranes. The first stage was to determine the ions concentration in the reservoir C_{salt}. Using the ionic Boltzmann distributions as in Eq. (13), one can get rid of the electrostatic energy

by multiplying the ions concentrations:

$$C_+(z) \times C_-(z) = C_{\text{salt}} \exp\left[-\beta eV(z) - \beta W_+(z)\right]$$
$$\times C_{\text{salt}}\left[\beta eV(z) - \beta W_-(z)\right]$$
$$= C_{\text{salt}}^2 \exp\left[-\beta\left(W_+(z) + W_-(z)\right)\right]. \quad (15)$$

In the reservoir, the ions concentration C_{salt} is constant. Moreover, one can also set $W_\pm = 0$ in the reservoir by defining the relative permittivity of the reservoir water as the reference value $\varepsilon_\perp^{\text{ref}}$ (Eq. (12)), which will be obtained in the second stage of the calibration. In the reservoir, Eq. (15) then gives:

$$C_{\text{salt}} = \sqrt{C_+ \times C_-} \quad (16)$$

Fig. S9 in the supplementary material shows the ionic concentrations in the most hydrated system at $T = 353.15\,\text{K}$, and the square root of their product which reaches indeed a constant value in the reservoir. The value of C_{salt} was then obtained by averaging the square root values in the reservoir.

Once this first step was done, we solved the mPB model's equation by following the method described in the precedent section II C, except we added the following constraint during the optimization process: $\varepsilon_\perp^{\text{plateau}} = \varepsilon_\perp^{\text{ref}}$. The dielectric permittivity indeed reached a plateau in the water region (where z values are close to z_{max}, as shown in Fig. 1). We identified this plateau value, which corresponds to the horizontal asymptote defined by the parameter $\varepsilon_\perp^{\text{plateau}}$ in Eq. (14), as the dielectric permittivity of the reservoir water. Since this parameter is optimized, the constraint allowed to maintain $W_\pm = 0$ in the reservoir, ensuring self-consistency with the first stage of the calibration procedure.

Finally, we kept the optimized value of $\varepsilon_\perp^{\text{plateau}}$ as the value of $\varepsilon_\perp^{\text{ref}}$ in all the systems at the same temperature.

III. RESULTS AND DISCUSSION

A. Resulting force between the bilayers

In stacked bilayers systems, the resulting force between lipid bilayers is the sum of three main contributions. The first one comes from the van der Waals interactions, which are attractive. The second one, the hydration repulsion, prevents the membranes from sticking to each others: it is a short-ranged interaction and decays exponentially with the thickness of the interlayer confined water[24]. The third one comes from the electrostatic interactions. In the case of charged lipid bilayers with monovalent salt, it is generally expected to be repulsive[25], but recent observations of DPPS membranes with NaCl salt suggest that this interaction could also be attractive[9].

For this reason, we first aimed at determining if the membranes in our simulations were attracting or repelling each others. The hydration forces between lipid bilayers can be extracted from MD simulations by calculating the water chemical potential[26,27]. In this work, we resorted to a different approach, valid for simulations without surface tension[28]. It involves looking at the Helmholtz free energy F, which depends on the volume V, the temperature T and the total number of particles N in the system. Smirnova and al. expressed, in the (NVT) ensemble, the excess of free energy ΔF, with respect to a single fully hydrated (in bulk water) lipid bilayer with no surface tension, as follows:

$$\Delta F = \Delta F_{\text{bilayer}} + \Delta F_{\text{water}} + g(d_{\text{w}})A , \qquad (17)$$

where $\Delta F_{\text{bilayer}}$ is the excess free energy contribution coming from the deformation of the bilayer, ΔF_{water} is the one coming from the deformation of the bulk of water surrounding the membrane, and g is the interface potential. This potential depends on the thickness of the interlayer water channel d_{w}, which can be estimated from the HN:

$$d_{\text{w}}(\text{HN}) = \frac{\text{HN} \times V_{\text{w}}}{A} , \qquad (18)$$

where $V_{\text{w}} = 29.7\,\text{Å}^3$ is the volume of a water molecule. We did not consider the dependence of this volume on the temperature here as we were not interested in quantitative measurements but rather in the qualitative behaviour in the simulation.

However our simulations were not carried at constant volume, but at constant pressure P in the (NPT) ensemble, meaning that the thermodynamic potential of interest would rather be the Gibbs free enthalpy G, which depends on P, T and N, with $\Delta G = \Delta F + P\Delta V$. Smirnova and al. stated that since the variation of the simulation box volume is negligible, then $\Delta G \approx \Delta F$. From there, they were able to express the repulsion pressure $P(d_{\text{w}})$ in the system, from the derivative of the interface potential g. Linking this to a change in the system's area, the repulsion pressure is given by:

$$P(d_{\text{w}}) = \frac{K_{\text{A}}}{d_{\text{w}}} \left(1 - \frac{A(d_{\text{w}})}{A_0} \right) , \qquad (19)$$

where A_0 is the reference area per lipid, which we took at the largest HN, and $A(d_{\text{w}})$ is the area per lipid for a given water thickness, i.e. a given HN. The behaviour between the membranes then just depends on the sign of this repulsion pressure. It will be repulsive if $P(d_{\text{w}}) > 0$ and attractive otherwise. In the end, it translates to a simple comparison between the area per lipid at a given HN and the area per lipid of reference taken at HN = 45. A higher area per lipid will denote an attractive behaviour while a smaller area per lipid will stand for a repulsion.

Fig. 2 shows the area per lipid as a function of the HN, at the five studied temperatures. It appears that at high
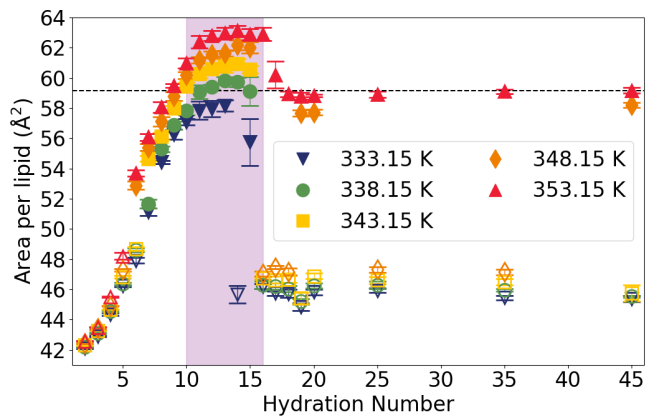
FIG. 2. Area per lipid *versus* hydration number at different temperatures. Filled markers represent bilayers in the fluid phase and open markers represent bilayers in the gel phase. The black dotted line shows the reference area per lipid A_0 at $T = 353.15\,\text{K}$. At this temperature, following Eq. (19), we identify the purple region as the hydration range at which the attractive behaviour appears.

HN (typically above 20), there is no significant change in the area per lipid upon dehydration. This indicates that in this HN range the bilayers are fully hydrated and they do not interact significantly. However, if we keep dehydrating the system, two thresholds appear. The first one is between HN = 20 and HN = 15. After it is reached, we see an increase in the area per lipid. The second threshold appears around HN = 10-11, below which the opposite phenomenon occurs: the area per lipid starts to decrease. These changes in the area per lipid can even induce phase transitions in the bilayers. In the coldest systems between HN = 20 and HN = 15, the bilayer undergoes a transition from the gel phase to the fluid phase. At lower HN, it undergoes a transition from the fluid phase to the gel phase in all the simulations.

Using Eq. (19), one has to take care of these phase changes when interpreting the differences in area per lipid. In this work, we can safely focus on the system at 353.15 K, as the bilayers stay in a fluid phase down to HN = 6. At high hydration, the system is in an equilibrium state and there is no significant force acting on the bilayers. However, after the first threshold is met, the area per lipid is higher than the reference value. This leads to a negative value for the repulsion pressure, thus indicating an attractive interaction between the bilayers. If the dehydration continues after the second threshold, the attractive behaviour stops. The bilayers start repelling each other as the area per lipid decreases under the reference value: the strong short-range repulsion, well identified in the literature for any kind of lipid bilayers[24], becomes dominant.

FIG. 3. Results from the modified Poisson Boltzmann model at 353.15 K, at HN = 35 (left) and HN = 10 (right). (a, d) Relative dielectric permittivity profile. (b, e) Reduced electric potential $\phi(z)$ and electric potential $V(z)$. (c, 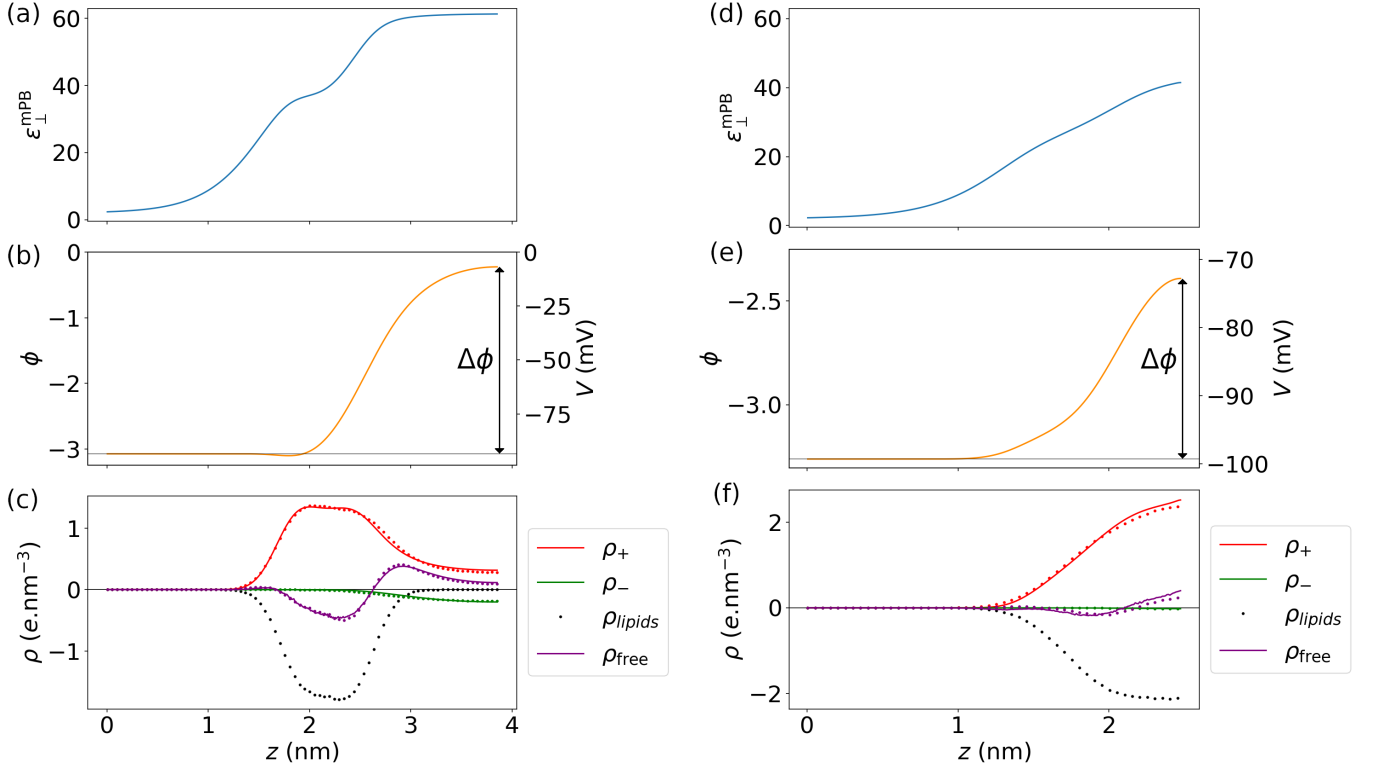f) Charge densities. Dots show data extracted from the MD simulation (for clarity, only one data point out of five is plotted), while lines show charge densities obtained with Eq. (13). Both purple plots include the lipid charge density extracted from the MD simulation.

B. Solutions of the mPB model and corresponding profiles

After the calibration was done, we were able to solve our model's equation (Eq. (S4) in the supplementary material). For each system, we obtained three profiles: the electric potential $V(z)$, the dielectric permittivity $\varepsilon_\perp^{\mathrm{mPB}}(z)$ and the ionic charge densities $\rho_\pm(z)$ predicted by the model (computed using the two latter and Eq. (13)). Example of these results for a DPPS bilayer at 353.15 K are shown in Fig. 3, both at high hydration (HN = 35, left side) and low hydration (HN = 10, right side). As illustrated in Fig. 1, thanks to the symmetry of the system, all plots are simplified to show only one half of the system. The lipid tails are located in the left side, the lipid heads are in the region where ρ_{lipids} is not null and the water is on the right side (with an overlap in the hydrophilic heads).

Fig. 3 (a, d) show the estimated relative dielectric permittivity profiles $\varepsilon_\perp^{\mathrm{mPB}}$ in the systems, obtained by inverting Eq. (14). The general shape of the profile naturally depends on the parametrized curve we chose to describe its inverse: one sigmoid and one Gaussian. In particular, thanks to the Gaussian component, the dielectric permittivity can display a small bump. This can notably be the case in the lipid heads region, where the structure is more complex because of the presence of free

charges (ions) and the complex distribution of charges and dipoles in the lipid heads. An example solution of the mPB model without the Gaussian component is given in Fig. S8 in the supplementary material to demonstrate its importance.

At high hydration number, the dielectric permittivity reaches a plateau in the confined interlayer water. This confirms that the bilayer is highly hydrated, therefore at the centre of the channel the water molecules are not constrained by the interactions with the lipids. With further dehydration however, this plateau is never reached, as seen in Fig. 3 (d). In this hydration state, all the remaining water molecules are located in the lipid heads region, where their orientation is somewhat constrained by electrostatic interactions, which is why a plateau is never reached.

Since the system is considered symmetrical with respect to the plane defined by $z = 0$ (other half of the bilayer, as visible in Fig. 1) and periodic through the MD periodic boundary conditions, we imposed when solving the model's equation that the derivative of the reduced electric potential is null at the borders to ensure its continuity, as visible in Fig. 3 (b).

For highly hydrated systems, we found a magnitude of about 100 mV for the electric potential difference ΔV between the lipid heads and the water, which corresponds to

$\Delta\phi \approx 3.3$. Though we did not manage to find an other value for a DPPS membrane in the literature to compare with the value given by the model, we found some values for a 1,2-dipalmitoyl-sn-glycero-3-phosphocholine (DPPC) membrane. This lipid has a different head than that of DPPS and is zwitterionic instead of being negatively charged. Stern and Feller carried out simulations of DPPC membranes and found a magnitude of around 1 V[29] ($\Delta\phi \approx 33$), while experimental values gave a smaller magnitude of 227 mV[30] ($\Delta\phi \approx 7.5$). One of the reasons the authors gave to explain such difference was the inaccuracy of the force field they used, which was CHARMM27[31]. Despite being a different lipid, we expected the order of magnitude of DPPS membrane's electric potential to be somewhat close from that of DPPC membrane. To strengthen this hypothesis, one can use Grahame equation[22], which derives from the standard Poisson-Boltzmann model and links the surface charge to the reduced surface potential, in the case of a planar solid wall:

$$\sinh\left(\frac{\Delta\phi}{2}\right) = \frac{2\pi\ell_B\lambda_D}{q}\frac{\sigma_s}{e}. \qquad (20)$$

Applied in our systems, where σ_s varies between 1 e per 0.4 to 0.6 nm^2 (depending on the area per lipid shown in Fig. 2), it gives a value $\Delta\phi \approx 4$, which is consistent with the value we measured. Since we used a much more recent version of the CHARMM force field than Stern and al., our results tend to validate their statement against the accuracy of CHARMM27.

With the profiles obtained in Fig. 3 (a) and (b), the model computes the ionic charge densities using Eq. (13). The results are shown in Fig. 3 (c) and compared with the charge densities obtained from the MD simulations. For both anions and cations, the charge densities computed by the model are in good agreement with MD data. In addition, since the solution for the electric potential appears to be consistent within the PB model, these results suggest that the profile of the dielectric permittivity $\varepsilon_\perp^{mPB}$ is a good approximation of the permittivity in the system.

C. Dielectric permittivity at the centre of the interlayer water channel

Once the mPB model has been solved in all systems, at all temperatures, one can extract the relative dielectric permittivities at the centre of the water channels by evaluating $\varepsilon_\perp^{mPB}(z_{max})$, where $z_{max} = L_z/2$ as shown in Fig. 1. The resulting values are plotted in Fig. 4 for bilayers in the fluid phase and in the gel phase.

The value at the centre of the water layer corresponds to the maximum of the dielectric permittivity profile. If one wanted to define an effective permittivity of the whole water slit, one would typically take the average of its inverse[32] $\varepsilon_\perp^{-1}$. Averaging over $\varepsilon_\perp^{-1}$ results in an effective permittivity that is dominated by the lower values
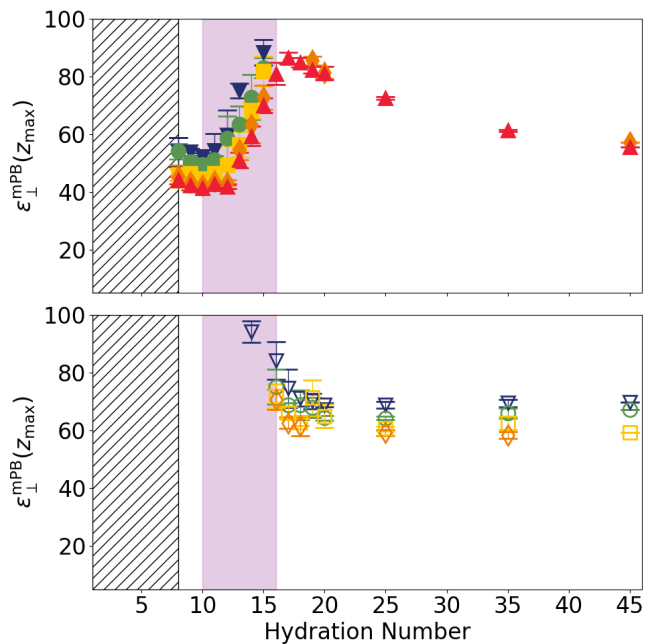
FIG. 4. Maximum dielectric permittivity *versus* hydration number at different temperatures, for bilayers in the fluid phase (top) and bilayers in the gel phase (bottom). The colours are the same as in Fig. 2 and the open/closed markers have the same meaning. The purple region represent where we identify an attractive regime between the membranes. The mPB model cannot be used in the hatched region because the ions no longer follow a Boltzmann distribution.

of $\varepsilon_\perp$. Therefore, a typical effective permittivity of the whole water slit would be lower than $\varepsilon_\perp^{mPB}$. The value of such an effective average of the dielectric permittivity strongly depends on the definition of its thickness and position, which are not easily defined in the case of lipid bilayers. We therefore resorted to investigate the maximum of the permittivity profiles.

At HN = 45, the values are in good agreement with the expected ones for the TIP3P model, in the presence of ions[33]. In the gel phase, the dielectric permittivity is rather constant upon dehydration while staying at high HN. However, it starts to raise at some point, which is counter-intuitive. The same phenomenon appears for the fluid phase, however in this case the raise seems to be continuous upon all the dehydration process. At the time we write this paper, we do not have a clear explanation for this increase. On the one hand, it could be because the real dielectric permittivity is actually a non-local property, but it is described as a local one in the model. In other words, $\varepsilon_\perp^{mPB}$ is an effective dielectric permittivity profile, optimized to describe the ionic charge densities, but not the real profile itself. It depends on the parametrized curve we chose to model it. Therefore, it is possible that this curves does not allow to describe the dielectric permittivity profile with enough accuracy and that the model compensates with odd values of the
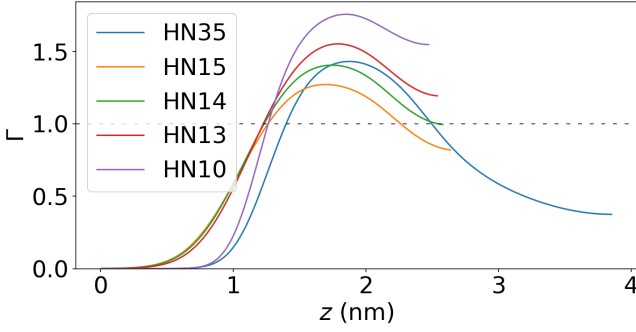
FIG. 5. Evolution of the plasma parameter at different HN. Above the dashed line at $\Gamma = 1$, ion correlations start to become non negligible.

dielectric permittivity. Given our choice of a smooth profile, we argue that our definition would be similar to the "coarse-grained dielectric constant" proposed by Borgis et al.[32]. This quantity, noted $\tilde{\varepsilon}_\perp(z)$, averaged over slices of the thickness of the same order of magnitude as a water molecule, is well-behaved and can be defined locally. Noticeably, in their study (Stockmayer fluid confined by Lennard-Jones planar walls[32]), this quantity also reaches a maximum well above the bulk value of the dielectric constant nearby the confining interface.

On the other hand, this increase could come from the mPB model itself. We brought two modifications to the standard PB model: we assumed a varying dielectric permittivity along the z axis and added the Born energy in the Boltzmann distribution of the ions. The model may lack some other interactions in this complex environment.

The purple region in Fig. 4 shows the HN range where we identified an attractive behaviour between the membranes. While the model gives high values of the dielectric permittivity when this behaviour arises, we observe a strong decrease of the dielectric permittivity, down to a plateau value at HN = 11 which is around half its value when the attraction arises. It is generally assumed that HN = 10 is a threshold value, corresponding to the water molecules bound to the lipid heads[34]. For this reason, the value of $\varepsilon_\perp^{\mathrm{mPB}}$ that remains close to 50 for the dehydrated systems (HN < 12) can be interpreted as the dielectric permittivity in lipid head region, that become almost independent of the water content.

Under HN = 8, the mPB model fails due to a lack of statistics. Because of the low number of anions and because the dynamics in the water channel between the membranes slows down a lot when reaching this dehydration state (even at high T), the charge density profile of the anions no longer follows a Boltzmann distribution.

D. Validity of the mPB model

It is known that PB theory is less accurate when approaching SC regime. To estimate when such electrostatic couplings may appear locally, one can compute the plasma parameter Γ, which compares the electrostatic interaction energy between two ions and the thermal energy. It is given by[7]:

$$\Gamma(z) = \frac{\ell_{\mathrm{B}}(z)}{d_{\mathrm{ion}}(z)} , \qquad (21)$$

where $d_{\mathrm{ion}}(z)$ is the typical distance between two ions and can be computed as follows: $d_{\mathrm{ion}}(z) = \sqrt[3]{C_+(z) + C_-(z)}$. The value $\Gamma = 1$ is the threshold at which correlations between the ions start to become non negligible[7,35]. Since these are not considered in the PB model, its accuracy decreases when Γ exceeds this value.

Fig. 5 shows the evolution of the plasma parameter in systems at $T = 353.15\,\mathrm{K}$, at different HN. At high hydration, the plasma parameter exceeds 1 in the lipid heads, but quickly decays to a lower value in the water. At HN = 14 and below, Γ stays over 1 in the water. Because of the correlations, the results given by the mPB model in this hydration range will be less accurate, though they can still be analysed qualitatively. In addition, the plasma parameter could be underestimated since it is computed using the dielectric permittivity given by the mPB model.

From their experimental study of DPPS membranes, Mukhina and al.[9] have made an estimation of the dielectric permittivity of the confined interlayer water. They found that values between 10 and 30 gave a coupling constant Ξ high enough to justify an attraction behaviour between the membrane in their system, within the SC theory. Their estimation of the dielectric constant took into account a measure of the interlayer water thickness, which corresponds to a HN between 8 and 10. The mPB model gives higher values for the dielectric permittivity at this hydration state, which could be caused by the discussed inaccuracies.

E. Comparison with alternative ways of estimating the relative dielectric permittivity

In this section, we compare the results obtained from the mPB model described in this work with alternative ways of estimating the dielectric permittivity.

Born dielectric permittivity— By getting rid of the electrostatic energy term the same way we did in Eq. (15), i.e. by multiplying the ionic concentrations, one can compute a dielectric permittivity profile $\varepsilon_\perp^{\mathrm{Born}}$ which would be the effective permittivity in the Born model. This "Born dielectric permittivity" derives from Eq. (12) and
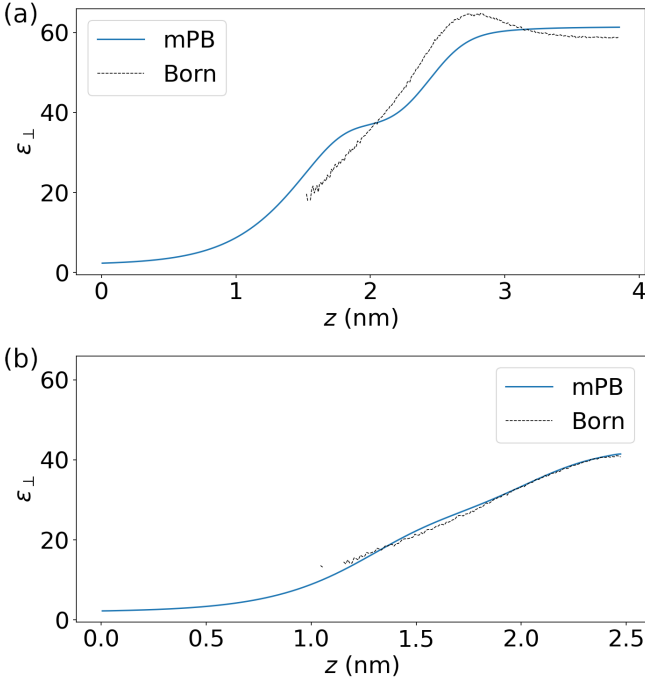
FIG. 6. Comparison between $\varepsilon_\perp^{\mathrm{mPB}}$ and $\varepsilon_\perp^{\mathrm{Born}}$ in systems at $T = 353.15\,\mathrm{K}$. (a) HN = 35. (b) HN = 10.

is given by:

$$
\frac{1}{\varepsilon^{\mathrm{Born}}(z)} = \frac{1}{\varepsilon_\perp^{\mathrm{ref}}} + \frac{16\pi\varepsilon_0}{\beta e^2}\frac{r_+ r_-}{r_+ + r_-}
$$
$$
\times \ln\left(\frac{C_{\mathrm{salt}}}{\sqrt{C_+(z) \times C_-(z)}}\right). \tag{22}
$$

Since the mPB model presented in this work highly relies on the Born model to compute the effective permittivity profile, comparing our results with the profile of $\varepsilon_\perp^{\mathrm{Born}}$ can give an insight on the self-consistence of the mPB model. Fig. 6 shows a comparison between $\varepsilon_\perp^{\mathrm{mPB}}$ and $\varepsilon_\perp^{\mathrm{Born}}$. Eq. (22) is not valid when the ionic concentrations are null, which is why $\varepsilon_\perp^{\mathrm{Born}}$ has no value in the tails region. Elsewhere however, it appears that the two profiles are quite similar, and even more at low HN.

Fluctuation-dissipation measurement— A classic way to estimate the dielectric permittivity in a medium is to use the fluctuation-dissipation theory and link the fluctuations of the water molecules' total dipole moment $\boldsymbol{M}$ to the dielectric permittivity[36]. In a homogeneous medium, this leads to:

$$
\varepsilon^{\mathrm{dip.\,fluct.}} = 1 + \frac{\langle M^2 \rangle - \langle M \rangle^2}{3\varepsilon_0 n_{\mathrm{w}} V_{\mathrm{w}} k_B T}, \tag{23}
$$

where n_{w} is the number of water molecules. Here we propose to estimate the dielectric permittivity through this formula, even though the system is not homogeneous.

Results of this method are shown in Fig. 7. At high hydration (HN $\geq$ 35), both mPB model and this method

give similar results. However, they differ more and more upon dehydration, because of two main reasons. The first one is that $\varepsilon^{\mathrm{dip.\,fluct.}}$ only takes into account the water molecules, while $\varepsilon_\perp^{\mathrm{mPB}}$ acts as an effective permittivity in the system, and does not strictly corresponds to the dielectric permittivity of the sole water molecules. The second reason is that by essence, $\varepsilon^{\mathrm{dip.\,fluct.}}$ is monotonically decreasing upon dehydration, as is is linked to the decrease of the rotational degree of freedom of water molecules. At very low HN, the only remaining water molecules are surrounded by charged components (being either the ions or the lipid heads). The dipole moment of the water molecules is then constrained by these interactions and cannot really fluctuate, explaining the extremely low values of the permittivity obtained with this method in such regime.

IV. CONCLUSION

We have presented a 1D modified Poisson-Boltzmann model, which allows the dielectric permittivity to vary along the axis and takes into account the solvation energy of the ions (Born energy) in their Boltzmann distribution.

In the model's equation, the two free charges densities come from the ions and from the lipids. The first one has an analytical description (a Boltzmann distribution) while the second one is added as an external fixed contribution obtained from MD simulations. Two unknowns remain in the equation: the electric potential and the dielectric permittivity. We left the electric potential as the unknown of the equation and we made an educated guess on the shape of the dielectric permittivity profile. With the help of a previous work that could compute this profile in systems without free charges only[12], we modelled

FIG. 7. Dielectric response of the water molecules *versus* hydration number for different temperatures. Black dots correspond to $\varepsilon_\perp^{\mathrm{mPB}}$ values at $353.15\,\mathrm{K}$. The colours are the same as in Fig. 2 and the open/closed markers have the same meaning. The purple region represent where we identify an attractive regime between the membranes.

the dielectric profile as a parametrized curve and optimized the parameters so that the analytical description of the ions in the model fitted at best the charge densities obtained from MD simulations.

Since this model can estimate the relative dielectric permittivity in a system containing free charges, we were able to use it to investigate water confined between charged lipid bilayers. The resul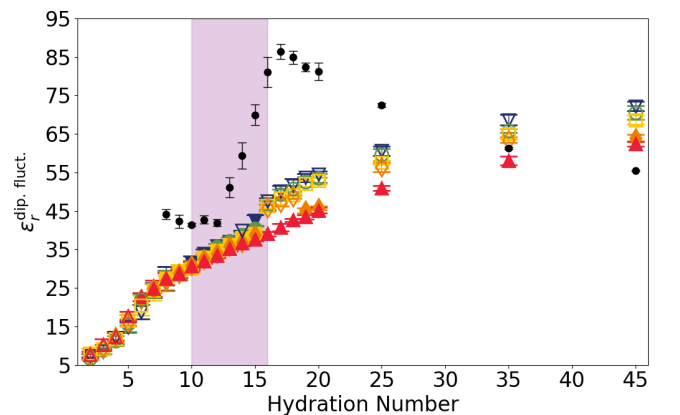ts show a self-consistence of the model, giving a dielectric permittivity profile close from the one that directly derives from the Born model. Moreover, when focusing on the dielectric permittivity at the centre of the interlayer channel, the mPB model shows a strong decrease of the dielectric constant when entering a hydration regime where the membranes attract each others. This observation is in agreement with the common interpretation of the phenomenon in the literature. At intermediate hydration levels, the mPB model results in local maximum of the dielectric constant that is higher than the bulk value. This may be due to the fact that our profiles are by construction smoothed, coarse-grained, and treat the dielectric permittivity as a local property. At high hydration, it is in good agreement with a classic way of computing the dielectric constant from the fluctuations of the water molecules dipole moment. However it diverges rather quickly from this method, which only considers the water molecules.

In the end, the model presented in this work is generic and thus can be applied in a large variety of systems where an electrolyte solution is confined between charged walls. We expect the mPB model to be more adapted to the simpler case of homogenous planar walls, as the thermal fluctuations of the membranes are not taken into account in the model (the lipid charge density profile is averaged over the simulation length). This model could also be useful to estimate the dielectric permittivity profile in biological systems, where the biological fluid of interest is not too much confined so the distributions of the salt it contains can be modelled with a Boltzmann distribution.

ACKNOWLEDGMENTS

AUTHOR DECLARATIONS

Conflict of interest— The authors have no conflict to disclose.

DATA AVAILABILITY

The data that support the findings of this study are available from the corresponding author upon reasonable request.

REFERENCES

[1] R. M. Forbes, A. R. Cooper, and H. H. Mitchell. The composition of the adult human body as determined by chemical analysis. *The Journal of biological chemistry*, 203:359–366, 1953.

[2] H. Binder. Water near lipid membranes as seen by infrared spectroscopy. *European Biophysics Journal*, 36:265–279, 2007.

[3] N. E. Levinger. Water in confinement. *Science*, 298:1722–1723, 2002.

[4] L. Fumagalli, A. Esfandiar, R. Fabregas, S. Hu, P. Ares, A. Janardanan, Q. Yang, B. Radha, T. Taniguchi, K. Watanabe, G. Gomila, K. S. Novoselov, and A. K. Geim. Anomalously low dielectric constant of confined water. *Science*, 360:1339–1342, 2018.

[5] N. Ben-Tal, B. Honig, R. M. Peitzsch, G. Denisov, and S. McLaughlin. Binding of small basic peptides to membranes containing acidic lipids: Theoretical models and experimental results. *Biophysical Journal*, 71:561–575, 1996.

[6] A. G. Moreira and R. R. Netz. Strong-coupling theory for counter-ion distributions. *Europhysics Letters*, 52:705–711, 2000.

[7] C. Herrero and L. Joly. The poisson-boltzmann equation in micro- and nanofluidics: A formulary. *Physics of Fluids*, 36, 2024.

[8] K. Komorowski, A. Salditt, Y. Xu, H. Yavuz, M. Brennich, R. Jahn, and T. Salditt. Vesicle adhesion and fusion studied by small-angle x-ray scattering. *Biophysical Journal*, 114:1908–1920, 2018.

[9] T. Mukhina, A. Hemmerle, V. Rondelli, Y. Gerelli, G. Fragneto, J. Daillant, and T. Charitat. Attractive interaction between fully charged lipid bilayers in a strongly confined geometry. *Journal of Physical Chemistry Letters*, 10:7195–7199, 2019.

[10] A. Schlaich, A. P. Dos Santos, and R. R. Netz. Simulations of nanoseparated charged surfaces reveal charge-induced water reorientation and nonadditivity of hydration and mean-field electrostatic repulsion. *Langmuir*, 35:551–560, 2019.

[11] G. Gramse, A. Dols-Perez, M. A. Edwards, L. Fumagalli, and G. Gomila. Nanoscale measurement of the dielectric constant of supported lipid bilayers in aqueous solutions with electrostatic force microscopy. *Biophysical Journal*, 104:1257–1262, 2013.

[12] A. Schlaich, E. W. Knapp, and R. R. Netz. Water dielectric effects in planar confinement. *Physical Review Letters*, 117, 2016.

[13] D. M. Huang, C. Cottin-Bizonne, C. Ybert, and L. Bocquet. Aqueous electrolytes near hydrophobic surfaces: Dynamic effects of ion specificity and hydrodynamic slip. *Langmuir*, 24:1442–1450, 2008.

[14] A. Poddar, D. Maity, A. Bandopadhyay, and S. Chakraborty. Electrokinetics in polyelectrolyte grafted nanofluidic channels modulated by the ion partitioning effect. *Soft Matter*, 12:5968–5978, 2016.

[15] S. Jo, T. Kim, V. G. Iyer, and W. Im. Charmm-gui: A web-based graphical user interface for charmm. *Journal of Computational Chemistry*, 29:1859–1865, 2008.

[16] J. B. Klauda, R. M. Venable, J. A. Freites, J. W. O'Connor, D. J. Tobias, C. Mondragon-Ramirez, I. Vorobyov, A. D. MacKerell, and R. W. Pastor. Update of the charmm all-atom additive force field for lipids: Validation on six lipid types. *Journal of Physical Chemistry B*, 114:7830–7843, 2010.

[17] W. L. Jorgensen, J. Chandrasekhar, J. D. Madura, R. W. Impey, and M. L. Klein. Comparison of simple potential functions for simulating liquid water. *The Journal of Chemical Physics*, 79:926–935, 1983.

[18] K. Vanommeslaeghe and A. D. Mackerell Jr. Charmm additive and polarizable force fields for biophysics and computer-aided drug design. *Biochimica et Biophysica Acta - General Subjects*, 1850:861–871, 2015.

[19] E. Duboué-Dijon, M. Javanainen, P. Delcroix, P. Jungwirth, and H. Martinez-Seara. A practical guide to biologically relevant molecular simulations with charge scaling for electronic polarization. *Journal of Chemical Physics*, 153, 2020.

[20] J. Melcr, T. M. Ferreira, P. Jungwirth, and O. H. S. Ollila. Improved cation binding to lipid bilayers with negatively charged pops by effective inclusion of electronic polarization. *Journal of Chemical Theory and Computation*, 16:738–748, 2020.

[21] M. J. Abraham, T. Murtola, R. Schulz, S. Páll, J. C. Smith, B. Hess, and E. Lindahl. Gromacs: High performance molecular simulations through multi-level parallelism from laptops to supercomputers. *SoftwareX*, 1-2:19–25, 2015.

[22] J. N. Israelachvili. *Intermolecular and Surface Forces (Third Edition)*. Academic Press, 2011.

[23] R. Schmid, A. M. Miah, and V. N. Sapunov. A new table of the thermodynamic quantities of ionic hydration: values and some applications (enthalpy–entropy compensation and born radii). *Physical Chemistry Chemical Physics*, 2:97–102, 2000.

[24] W. Xu and F. Pincet. Quantification of phase transitions of lipid mixtures from bilayer to non-bilayer structures: Model, experimental validation and implication on membrane fusion. *Chemistry and Physics of Lipids*, 163:280–285, 2010.

[25] J. Marra. Direct measurement of the interaction between phosphatidylglycerol bilayers in aqueous electrolyte solutions. *Biophysical Journal*, 50:815–825, 1986.

[26] E. Schneck, F. Sedlmeier, and R. R. Netz. Hydration repulsion between biomembranes results from an interplay of dehydration and depolarization. *Proceedings of the National Academy of Sciences of the United States of America*, 109:14405–14409, 2012.

[27] A. Schlaich, J. O. Daldrop, B. Kowalik, M. Kanduč, E. Schneck, and R. R. Netz. Water structuring induces nonuniversal hydration repulsion between polar surfaces: Quantitative comparison between molecular simulations, theory, and experiments. *Langmuir*, 40:7896–7906, 2024.

[28] Y. G. Smirnova, S. Aeffner, H. J. Risselada, T. Salditt, S. J. Marrink, M. Müller, and V. Knecht. Interbilayer repulsion forces between tension-free lipid bilayers from simulation. *Soft Matter*, 9:10705–10718, 2013.

[29] H. A. Stern and S. E. Feller. Calculation of the dielectric permittivity profile for a nonuniform system: Application to a lipid bilayer simulation. *Journal of Chemical Physics*, 118:3401–3412, 2003.

[30] K. Gawrisch, D. Ruston, J. Zimmerberg, V. A. Parsegian, R. P. Rand, and N. Fuller. Membrane dipole potentials, hydration forces, and the ordering of water at membrane surfaces. *Biophysical Journal*, 61:1213–1223, 1992.

[31] S. E. Feller and A. D. MacKerell. An improved empirical potential energy function for molecular simulations of phospholipids. *Journal of Physical Chemistry B*, 104:7510–7515, 2000.

[32] D. Borgis, D. Laage, L. Belloni, and G. Jeanmairet. Dielectric response of confined water films from a classical density functional theory perspective. *Chemical Science*, 14:11141–11150, 2023.

[33] S. Izadi, R. Anandakrishnan, and A. V. Onufriev. Building water models: A different approach. *Journal of Physical Chemistry Letters*, 5:3863–3871, 2014.

[34] S. Malik and A. Debnath. Dehydration induced dynamical heterogeneity and ordering mechanism of lipid bilayers. *Journal of Chemical Physics*, 154, 2021.

[35] Y. Levin. Electrostatic correlations: from plasma to biology. *Reports on Progress in Physics*, 65:1577–1632, 2002.

[36] J. G. Kirkwood. The dielectric polarization of polar liquids. *The Journal of Chemical Physics*, 7:911–919, 1939.

Appendix S-I: Numerical solving of the mPB model

A custom Python code has been written to solve the mPB model. It is available here: `https://github.com/lgardre/mPB.git`. Let us develop Eq. (11), using Eqs. (12) and (13):

$$\frac{\mathrm{d}^2\phi}{\mathrm{d}z^2} = \frac{\beta e^2}{\varepsilon_0 \varepsilon_\perp(z)}\left\{ C_{\mathrm{salt}}\left(\mathrm{e}^{-\beta W_-(z)+\phi(z)} - \mathrm{e}^{-\beta W_+(z)-\phi(z)} \right) + n_{\mathrm{lipids}}(z) \right\} - \frac{1}{\varepsilon_\perp(z)}\frac{\mathrm{d}\varepsilon_\perp(z)}{\mathrm{d}z}\frac{\mathrm{d}\phi(z)}{\mathrm{d}z}, \tag{S1}$$

with $\rho_{\mathrm{lipids}}(z) = -e\, n_{\mathrm{lipids}}(z)$.

To solve this equation, we use the `solve_bvp()` function from `scipy.integrate`. However, this function can only solve first order ODEs. Let us then rewrite Eq. (11) as a system of first order ODEs. We define $\phi_1(z)$ and $\phi_2(z)$ as follows:

$$\phi_1(z) = \phi(z) \text{ and } \phi_2(z) = \frac{\mathrm{d}\phi_1(z)}{\mathrm{d}z} = \frac{\mathrm{d}\phi(z)}{\mathrm{d}z}. \tag{S2}$$

The system of equations then follows:

$$\begin{cases} \dfrac{\mathrm{d}\phi_1(z)}{\mathrm{d}z} = \phi_2(z) \\ \dfrac{\mathrm{d}\phi_2(z)}{\mathrm{d}z} = \dfrac{\beta e^2}{\varepsilon_0 \varepsilon_\perp(z)}\left\{ C_{\mathrm{salt}}\left(\mathrm{e}^{-\beta W_-(z)+\phi_1(z)} - \mathrm{e}^{-\beta W_+(z)-\phi_1(z)} \right) + n_{\mathrm{lipids}}(z) \right\} - \dfrac{1}{\varepsilon_\perp(z)}\dfrac{\mathrm{d}\varepsilon_\perp(z)}{\mathrm{d}z}\phi_2(z) \end{cases}. \tag{S3}$$

We then introduce the inverse of the dielectric permittivity $\varepsilon_\perp^{-1}(z)$, so we rewrite Eq. (S3) accordingly:

$$\begin{cases} \dfrac{\mathrm{d}\phi_1(z)}{\mathrm{d}z} = \phi_2(z) \\ \dfrac{\mathrm{d}\phi_2(z)}{\mathrm{d}z} = \dfrac{\beta e^2}{\varepsilon_0}\varepsilon_\perp^{-1}(z)\left\{ C_{\mathrm{salt}}\left(\mathrm{e}^{-\beta W_-(z)+\phi_1(z)} - \mathrm{e}^{-\beta W_+(z)-\phi_1(z)} \right) + n_{\mathrm{lipids}}(z) \right\} + \dfrac{1}{\varepsilon_\perp^{-1}(z)}\dfrac{\mathrm{d}\varepsilon_\perp^{-1}(z)}{\mathrm{d}z}\phi_2(z) \end{cases}. \tag{S4}$$

Appendix S-II: Inverse dielectric permittivity profile and role of the Gaussian
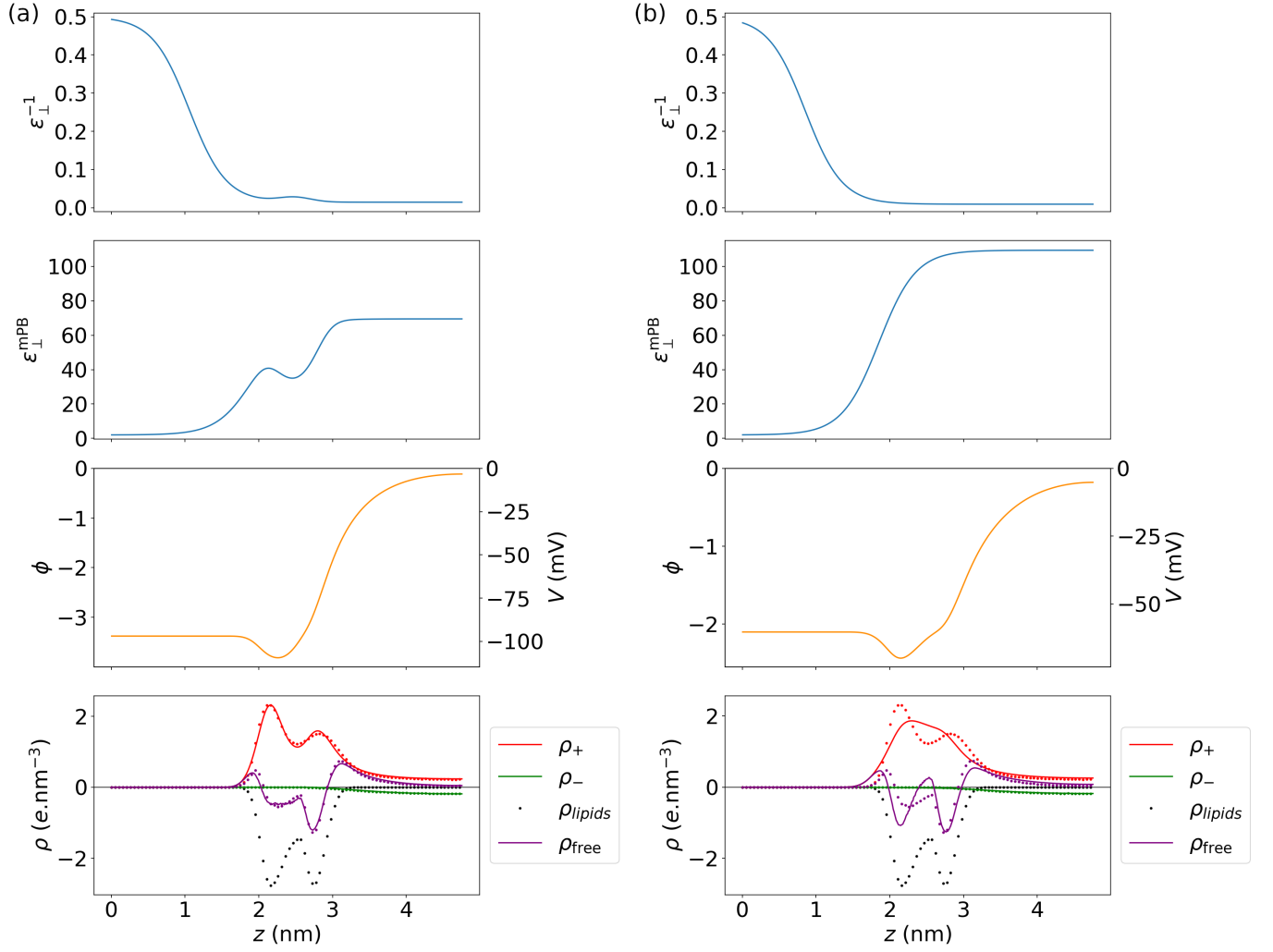

FIG. S8. Results from the modified Poisson Boltzmann model at $HN = 35$ and $T = 333.15\,\mathrm{K}$ (lipid bilayer in the gel phase). (a) The inverse of the dielectric permittivity is modelled with a sigmoid and a Gaussian. (b) The inverse of the dielectric permittivity is only modelled with a sigmoid.

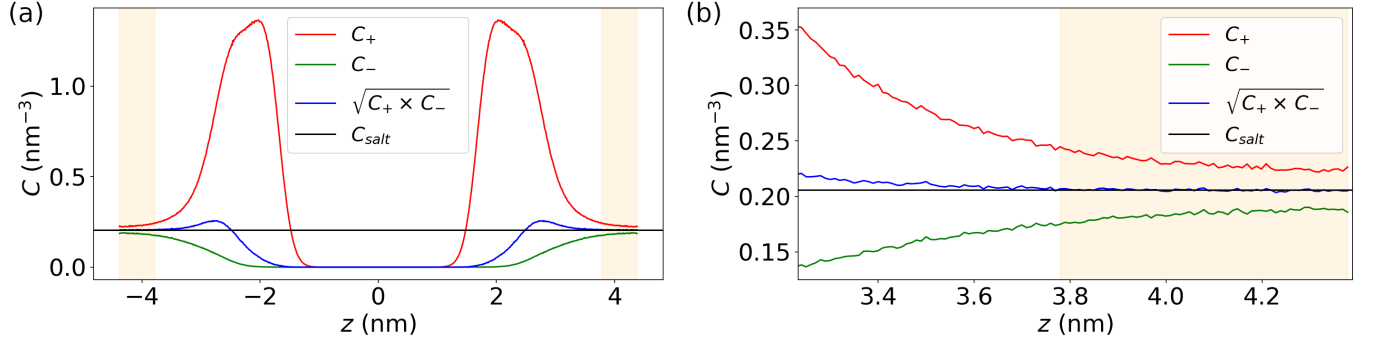**Appendix S-III: Details about the calibration of the mPB model**

FIG. S9. First step of the calibration on the system at HN $= 45$ and $T = 353.15\,\mathrm{K}$. (a) Ionic concentrations in the system. The salt concentration, given by Eq. (16), is constant in the highlighted regions. (b) Zoom on a highlighted region. The constant C_salt is obtained by averaging the values of the salt concentration in both highlighted regions.

T (K)	C_salt (nm^{-3})	$\varepsilon_\perp^\mathrm{ref}$
$333.15\,\mathrm{K}$	0.187 ± 0.002	69.816 ± 1.693
$338.15\,\mathrm{K}$	0.184 ± 0.003	67.303 ± 1.693
$343.15\,\mathrm{K}$	0.182 ± 0.003	59.309 ± 1.430
$348.15\,\mathrm{K}$	0.209 ± 0.002	57.198 ± 1.523
$353.15\,\mathrm{K}$	0.206 ± 0.002	55.514 ± 1.616

TABLE S1. Calibration values